Procedia Manufacturing

Volume 5, 2016, Pages 427–441

44th Proceedings of the North American Manufacturing Research Institution of SME http://www.sme.org/namrc

Productivity Progression with Tool Wear in Titanium Milling

Joyson Menezes, Mark A. Rubeo, Kadir Kiran, Andrew Honeycutt, and Tony L. Schmitz

University of North Carolina at Charlotte, Charlotte, NC

jmenezes@uncc.edu, mrubeo@uncc.edu, kkiran@uncc.edu, ahoney15@uncc.edu, tony.schmitz@uncc.edu

Abstract

This paper presents experimental results for flank wear width, cutting force, temperature, and surface finish with increasing tool wear in titanium (Ti6Al4V) milling. The variation in these process indicators is presented for repeated trials as the wear progresses from a new tool condition to a significantly worn state. Based on the measured force data, cutting force coefficients are determined using a nonlinear optimization algorithm as the tool wears and these coefficients are combined with the structural dynamics to predict the process stability. The achievable chatter-free material removal rate is then computed for both the new and worn tool conditions. In this way, the variation in productivity is related to the wear state. As expected, the productivity reduces with increase wear.

Keywords: Milling, wear, force, temperature, surface finish, stability, chatter

1 Introduction

Titanium represents an important material for the aerospace and medical industries, as well as the automotive and energy fields. Subsequently, there is widespread interest in high productivity machining strategies. A significant limitation to high material removal rates when machining Ti6Al4V, a popular titanium alloy, is its low thermal conductivity. For comparison, Ti6Al4V conductivity is approximately 7 N/(s-^{o}C), while 1045 steel is 43 N/(s-^{o}C) and 7075-T6 aluminum is 140 N/(s-^{o}C) (Tlusty, 1999). Although the shear plane temperature is similar when machining Ti6Al4V and 1045 steel, the significant reduction in thermal conductivity for titanium causes the heat to be localized at the tool-chip interface and diffusive (temperature-driven) tool wear is accelerated. Because the cutting temperature tends to increase with cutting speed, low speeds are typically selected to ensure adequate tool life. These low cutting speeds result in relatively lower material removal rates (MRR).

Selection and peer-review under responsibility of the Scientific Programme Committee of NAMRI/SME

doi:10.1016/j.promfg.2016.08.036

Titanium machining research efforts have studied, for example, tool wear mechanisms, including diffusion and adhesion thermo-chemical reactions (Hartung & Kramer, 1982), high speed cutting strategies (Abele & Fröhlich, 2008), and cryogenic machining (Hong et al., 2001). It has been observed that choosing cutting tools with many teeth (10 or more) can increase material removal rate while maintaining small feed per tooth values, low radial immersions, and high axial depths of cut. The associated challenge is efficient chip evaluation. The selection of tool paths that maintain a constant radial depth of cut has also been suggested to increase tool life (Zelenski, 2012). Other related tool wear evaluation efforts include Remadna & Rigal, 2006, Nouari & Ginting, 2006, Castejóna et al., 2007, Kuttolamadom et al. 2012a and 2012b, Sun et al., 2014, and Niaki et al., 2015.

In this paper, a study is described where the tool wear, cutting zone temperature, cutting force, and machined surface roughness were monitored over the life of a cutting tool while milling Ti6Al4V. The trends in these important process indicators are reported for multiple cutting trials. Additionally, the cutting force signal is used to estimate the cutting force coefficients by a nonlinear optimization approach as the tool wears. The change in force coefficients is used together with the system dynamics to identify the change in achievable MRR with wear state considering the limitation imposed by unstable machining conditions, or chatter. The paper is organized as follows. First, the experimental setup, which includes tool wear, temperature, force, and machined surface finish measurements, is detailed. Next, the nonlinear optimization procedure for cutting force coefficient determination is described. Then, the experimental results are presented and trends are highlighted. Finally, the MRR is calculated given the combined limitations imposed by tool wear and chatter.

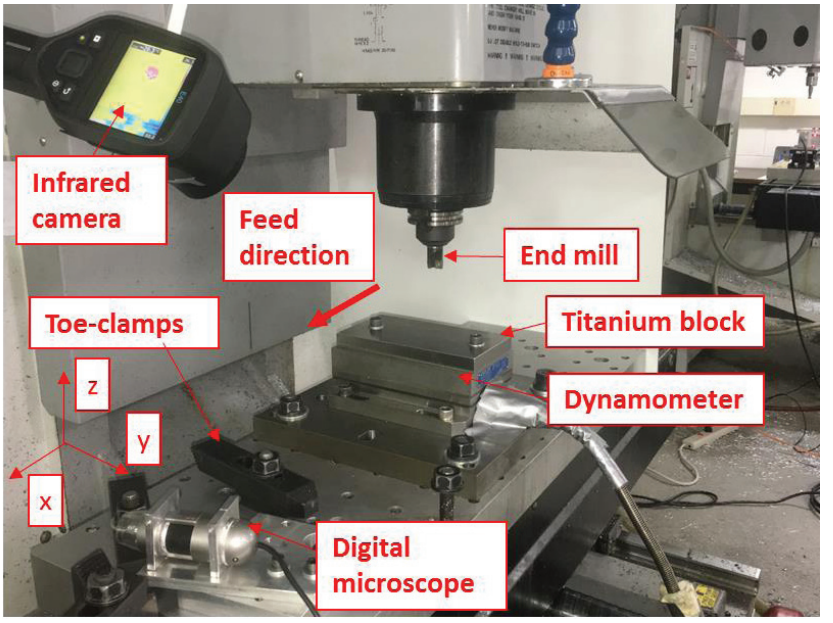

Figure 1. Setup for cutting force, tool wear, and temperature measurements using three-axis dynamometer, digital microscope, and infrared camera.

2 Experimental Setup

Cutting tests were performed on a Haas TM-1 computer numerically-controlled (CNC) vertical milling machine with a maximum spindle speed of 4000 rpm. The workpiece material was Ti6Al4V with approximate dimensions of 167 mm × 87 mm × 15.4 mm. The workpiece was rigidly fixed to a

three-component cutting force dynamometer (Kistler 9257B) using two M8 socket head cap screws; see Figure 1. The dynamometer/workpiece combination was bolted to the machine tool's table via a surface ground steel plate approximately 25 mm in thickness and was aligned to the machine axes using a dial indicator. A charge amplifier (Kistler Type 5010), data sampling interface, (Data Translation DT9837B), and acquisition software (Spinscope, Manufacturing Laboratories Inc.) were used to record the cutting force. A portable digital microscope (Dino-Lite model Pro-AM4137) with 60× magnification and collection/analysis software DinoCapture 2.0 (AnMo Electronics Corp.) were used to record the flank wear width (FWW) at regular intervals. The digital microscope was clamped to the machine table; for each tool measurement, the tool was positioned in the same location and the "orient spindle" CNC command was used to set the cutting edge to a repeatable measurement location and orientation.

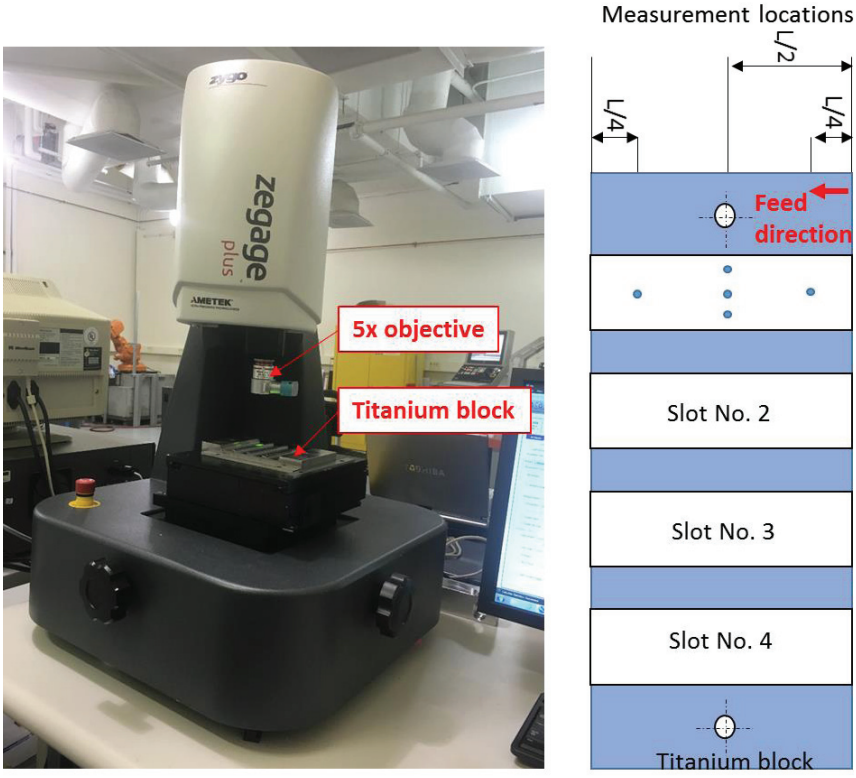

Figure 2. Setup for surface roughness measurements using ZeGage Plus 3D optical profiler (left), and measurement locations for each slot (right).

A FLIR E40 infrared camera (FLIR Systems, Inc.) was used to measure the cutting temperature (160×120 pixels). The temperature range used in the measurements was zero to 650°C. At least four infrared images were captured during each cutting trial and the maximum temperature was recorded as the cutting temperature. Because the integration time for the temperature measurement was larger than the time for each tooth passage, the reported temperatures can be considered to be average values and used only to indicate trends in the machining process. After each trial and associated tool wear, temperature, and cutting force measurements, the surface roughness was measured using a ZeGage Plus 3D optical profiler with a 5× objective. In order to measure the surface roughness, the workpiece was removed from the dynamometer, mounted on the profiler, and measured

at five location points for each machined slot; see Figure 2. After the surface roughness measurements, the workpiece was again bolted to the dynamometer and prepared for the next test cut by facing the workpiece with a separate tool to ensure the top surface was parallel with the machine table.

The cutting tool used in this study was a single tooth, 19.1 mm diameter indexable square endmill (Cutting Tool Technologies model DRM-03) with PVD-coated (TiN/TiCN/TiN) carbide inserts (SPEB322 KC725M). The inserts had no edge preparation, an 11° relief angle, a 0.8 mm nose radius, and 0° rake and helix angles. The insert was clamped in a Valenite® (V40CT-E75-175) tool holder with approximately 28 mm of overhang.

Cutting tests were performed under stable and dry milling conditions with a 100% radial immersion (slot milling), a cutting speed of 50 mm/min, an axial depth of cut of 2.7 mm, a spindle speed of 835 rpm, and a feed per tooth of 0.1 mm/tooth. Eight slots were machined for each insert.

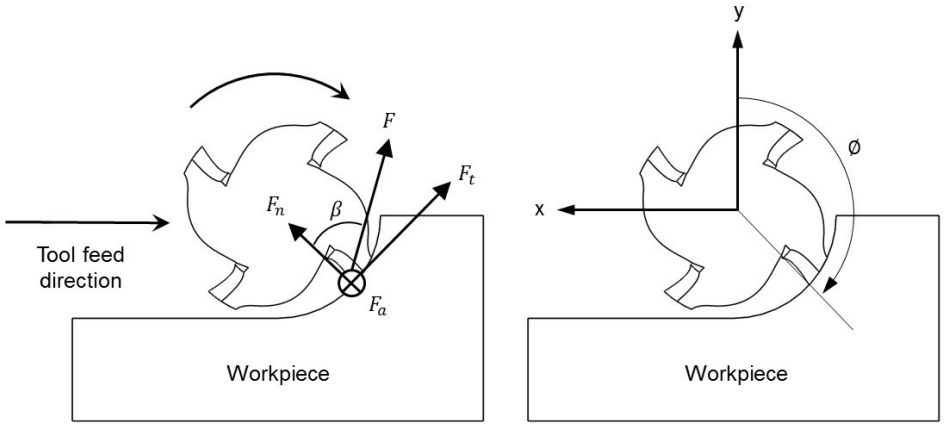

Figure 3. Force components and fixed reference frame for the optimization method.

3 Cutting Force

The mechanistic force model applied in this research was based on the assumptions that: 1) the instantaneous cutting force is proportional to the cross sectional area of the uncut chip through empirical cutting force coefficients; and 2) the instantaneous cutting forces are independent of other machining parameters. Although this assumption provides a reasonable degree of accuracy for milling stability prediction using stability lobe diagrams (Schmitz & Smith, 2008), it has been shown that cutting forces are also dependent on cutting speed and feed (Campatelli & Scippa, 2012). The mechanistic force model used in this study includes instantaneous cutting forces in the tangential, F_t, and normal, F_n, and axial, F_a, directions (Figure 3) and six corresponding cutting force coefficients; see Equations 1-3 (Altintas, 2012):

$$F_t = k_{tc} bh + k_{te} b \tag{1}$$

$$F_n = k_{nc} bh + k_{ne} b \tag{2}$$

$$F_a = k_{ac} bh + k_{ae} b \tag{3}$$

where b is the chip width (i.e., axial depth of cut in milling) and h is the instantaneous chip thickness, which is based on the circular tooth path approximation; see Equation (4):

$$h = f_t \sin(\phi) \tag{4}$$

where f_t is the feed per tooth and ϕ is the cutter rotation angle. Each component of the instantaneous cutting force includes two cutting force coefficients. The coefficients k_{tc}, k_{nc}, and k_{ac} are correlated with cutting and the edge coefficients k_{te}, k_{ne}, and k_{ae} are correlated with ploughing. The edge coefficients affect the instantaneous cutting force proportionally through the chip width, but are independent of the instantaneous chip thickness.

The Ti6Al4V cutting force coefficients were identified in this study using an instantaneous force, nonlinear optimization method which solves a nonlinear, least squares curve fitting problem and takes into account the user-defined lower and upper bounds on the decision variables (i.e., cutting force coefficients). The optimization routine, which uses a trust-region-reflective least squares algorithm, equates cutting forces simulated in the time domain with measured cutting forces at each discrete time step. This approach offers an advantage over the more traditional linear regression approach, where a linear fit to the mean force components recorded over several feed per tooth values is used to determine the coefficients (Schmitz & Smith, 2008). In the nonlinear optimization approach, only a single cutting force signal is required and multiple cuts are not necessary. In the case of Ti6Al4V machining where tool wear is an issue, the optimization approach was a preferred alternative.

The time domain simulation embedded within the optimization algorithm calculates the cutting forces at each small time step, dt, which is defined in the simulation as:

$$dt = \frac{1}{f_s} \tag{5}$$

where f_s is the sampling frequency for the cutting force measurement. At each time step the instantaneous chip thickness is computed, the cutting force is calculated, the tooth angle, ϕ, is incremented by a small angle, $d\phi$, which depends on the spindle speed and the time step, and the process is repeated for one complete revolution of the cutting tool. The instantaneous chip thickness is determined using the circular tooth path approximation and a rigid tool and workpiece is assumed (although this is not strictly required).

The tangential, F_t, normal, F_n, and axial, F_a, cutting force components (see Figure 3) are calculated according to the mechanistic force model defined in Equations 1-3. In order to represent the simulated forces in the fixed reference frame of the measured cutting forces, a coordinate transformation is performed:

$$\begin{Bmatrix} F_x \\ F_y \\ F_z \end{Bmatrix}_{simulated} = \begin{bmatrix} \cos(\phi) & \sin(\phi) & 0 \\ \sin(\phi) & -\cos(\phi) & 0 \\ 0 & 0 & 1 \end{bmatrix} \begin{Bmatrix} F_t \\ F_n \\ F_a \end{Bmatrix}_{simulated} \tag{6}$$

where ϕ is the instantaneous cutter rotation angle. The objective function is defined as:

$$f_i(k) = \begin{Bmatrix} F_x \\ F_y \\ F_z \end{Bmatrix}_i^{simulated} - \begin{Bmatrix} F_x \\ F_y \\ F_z \end{Bmatrix}_i^{measured} \tag{7}$$

where k is the vector of decision variables, which includes the six cutting force coefficients and $f_i(k)$ is the difference between the x, y, and z components of the instantaneous simulated and measured cutting forces at the ith time step.

Because the time step between each simulated instantaneous cutting force must coincide with the measured cutting forces, the size of the resulting system of equations depends on the sampling

frequency of the measurement and the number of cutting tool revolutions (i.e., number of time steps) included in the optimization. The nonlinear, least squares curve fitting problem takes the form:

$$\min_k \|f(k)\|_2^2 = \min_k (f_1(k)^2 + f_2(k)^2 + \cdots + f_n(k)^2) \tag{8}$$

where n is the number of time steps. The curve fitting problem is solved via a trust-region-reflective algorithm, which is based on an interior-reflective Newton approach that is well-suited to solving nonlinear optimization problems where the decision variables are bounded by upper and/or lower limits (Coleman & Li, 1994).

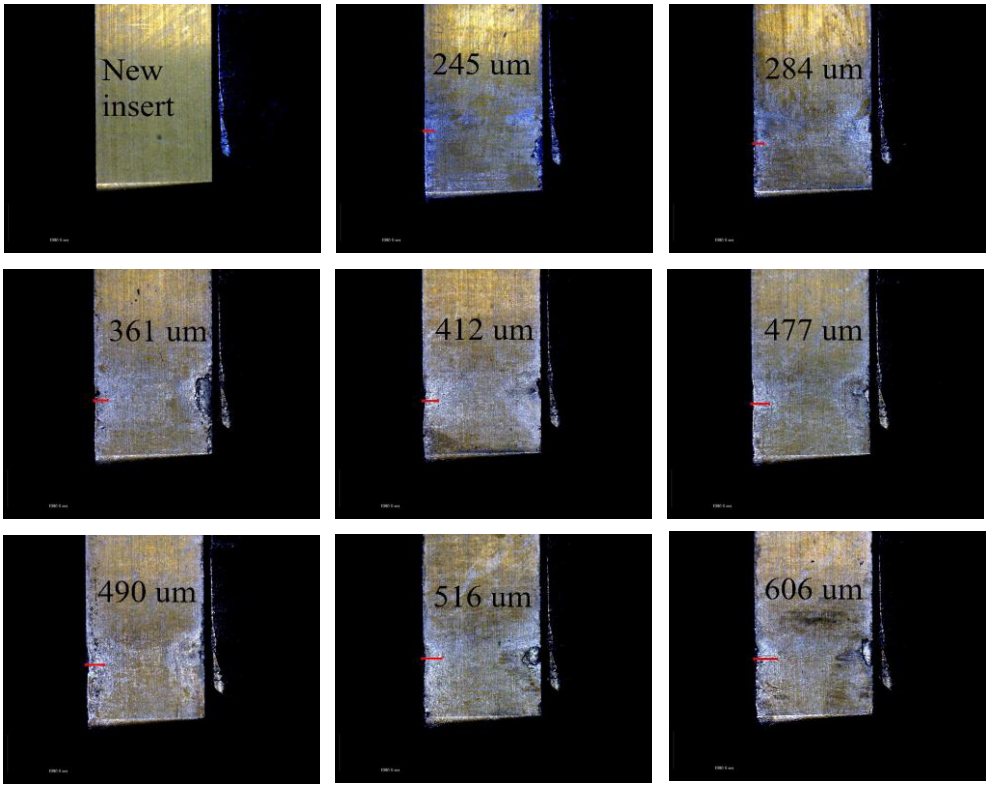

Figure 4. FWW progression per machined slot in one cutting trial (new tool and eight slots). The images were collected using the digital microscope. In the images, the rake face is on the left and the flank face is shown. The numerical FWW values are included, as well as the maximum FWW measurement location (horizontal line).

For this study, the measured cutting forces were partitioned into 100 individual revolutions of the cutting tool and averaged. The measured cutting forces exhibited a high degree of repeatability from one revolution of the cutting tool to the next. The average measured cutting force components were then used for the nonlinear optimization function along with a number of relevant process parameters, including the number of teeth on the cutting tool, sampling frequency of the force measurement, and initial guesses for the decision variables (i.e., cutting force coefficients).

The optimization function simulates the instantaneous cutting forces in the x, y, and z directions based on the input process parameters. The difference between the simulated and measured cutting forces is then calculated by the objective function and the sum of squares of the differences is evaluated. The evaluation is then examined against an arbitrary, user-defined set of convergence

criteria, such as the change in the sum of the squares from one iteration to the next. If it is determined that the convergence criteria are met, the optimization routine ceases; otherwise, the decision variables are updated and the process iterates until convergence.

4 Experimental Results

In this section, the changes in FWW, cutting force, cutting temperature, and machined surface finish with progressive tool wear are presented. The experimental results are shown and trends are identified. In each case, the mean results and ± two standard deviation error bars from four sets of eight slots (a new insert was used for each set) are presented.

4.1 Tool Wear

After each slot was machined, the FWW was measured. As noted, a total of eight slots were produced for each insert and four trials were completed. Figure 4 shows the FWW progression for one insert. The results are typical of all four independent trials. The maximum FWW was recorded for each slot and the results are summarized in Figure 5. In this figure the mean maximum FWW and ± two standard deviation (95%) error bars are plotted versus the slot number. The volume per slot is approximately 4487 mm^3 (87 mm × 2.7 mm × 19.1 mm). As expected, the FWW grows with increasing cutting time/volume.

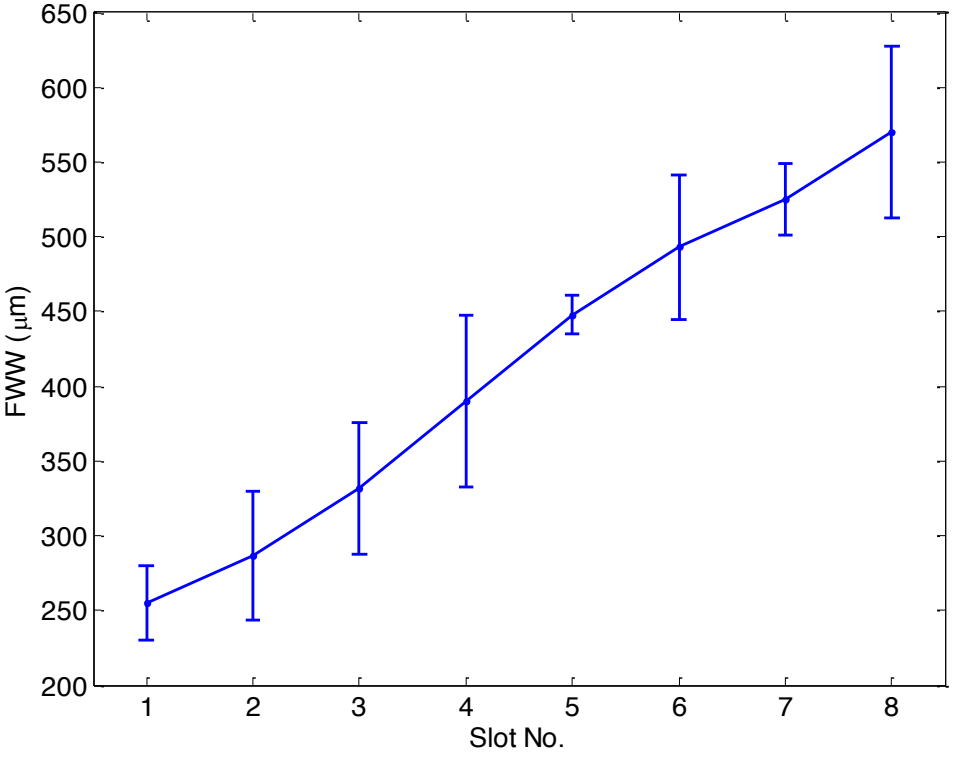

Figure 5. Maximum FWW progression per machined slot for all four trials. The mean and ± two standard deviation error bars are shown.

4.2 Cutting Force

The time-domain cutting force components (x, y, and z directions) were measured and the optimization algorithm was then used to identify the cutting force coefficients and their change with tool wear after each slot. Example results are presented in Figures 6 and 7. Figure 6 shows the x and y direction force components from 100 consecutive cutting revolutions. Figure 7 displays an example fitting result for the same data. The subsequent changes in the force are presented in Figures 8-11.

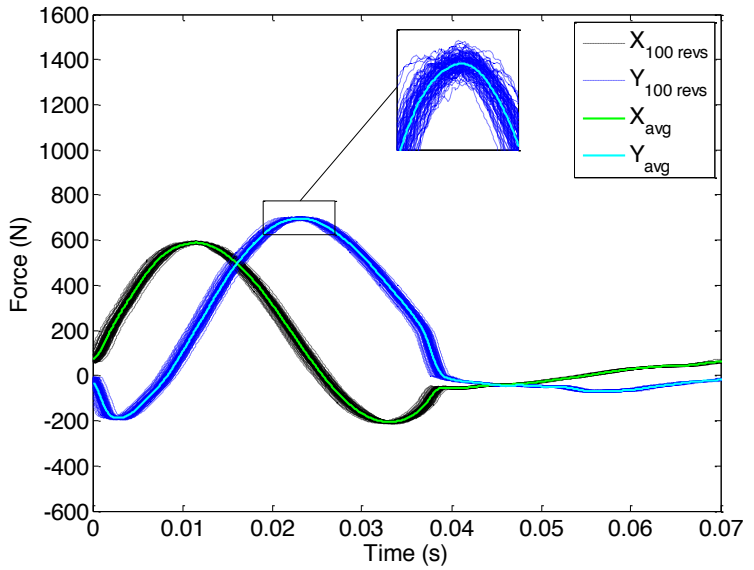

Figure 6. Example force measurement for 100 revolutions with the mean x and y components.

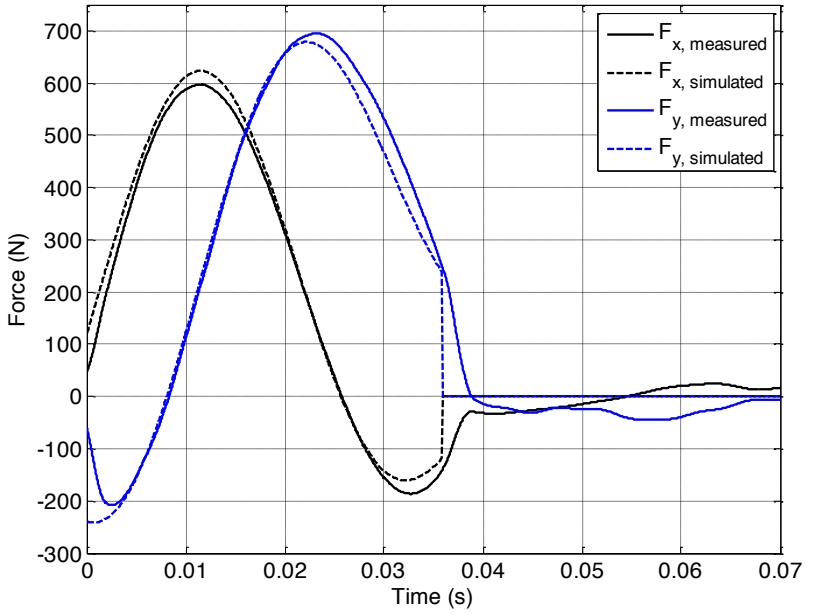

Figure 7. Example fitting result from the nonlinear optimization algorithm using the Figure 6 data.

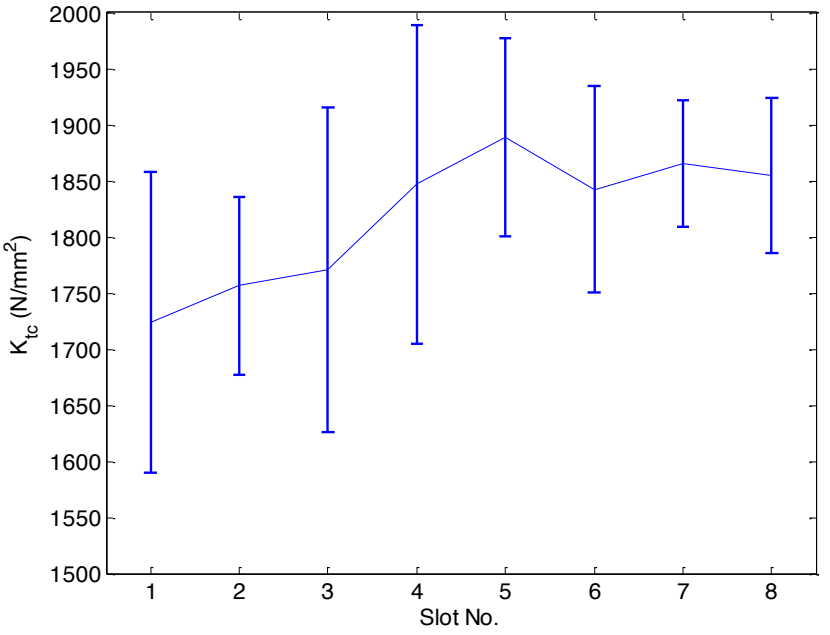

Figure 8. Tangential cutting force coefficient progression per machined slot for all four trials.

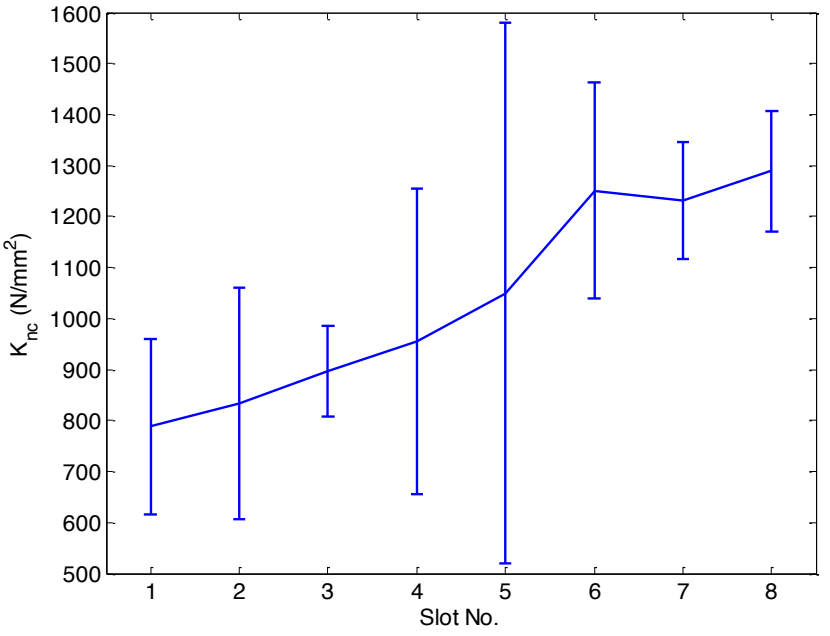

Figure 9. Normal cutting force coefficient progression per machined slot for all four trials.

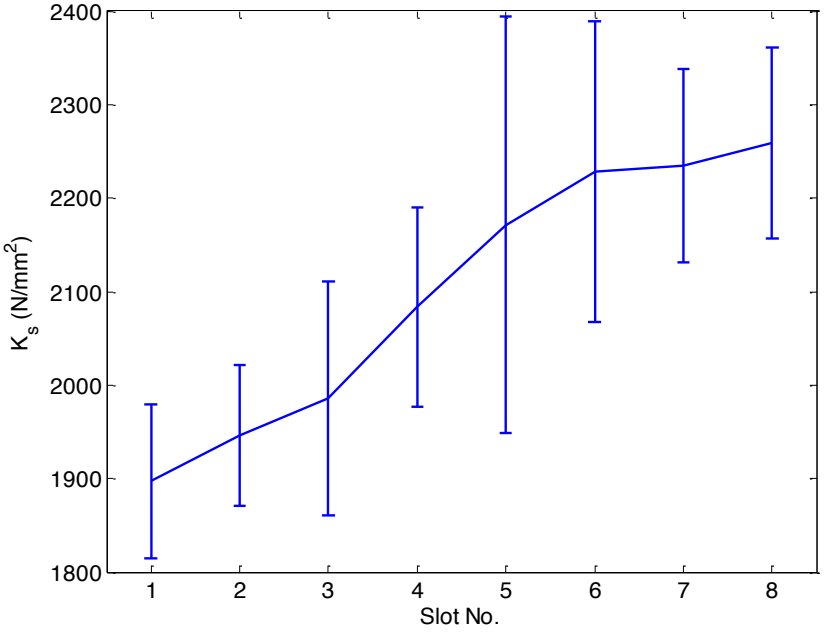

Figure 10. Specific cutting energy progression per machined slot for all four trials.

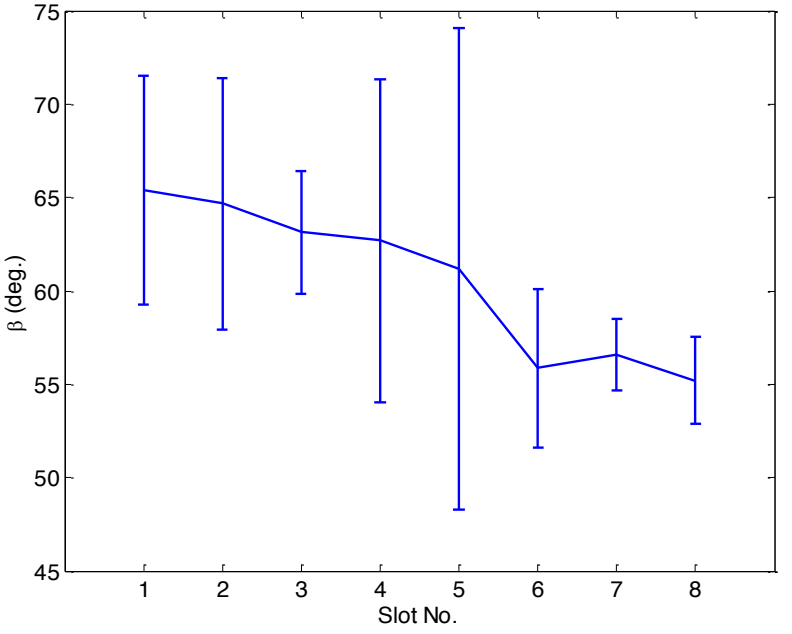

Figure 11. Resultant force angle progression per machined slot for all four trials.

The tangential and normal direction cutting force coefficients are displayed in Figures 8 and 9. The larger percent growth in the normal cutting coefficient indicates that, as the tool wears, the resultant

cutting force is rotated toward the surface normal as its magnitude grows. This behavior is captured in Figures 10 and 11. Figure 10 displays the specific cutting force, $K_s = \sqrt{{k_{tc}}^2 + {k_{nc}}^2}$. The growth in K_s indicates the increase in resultant force. Figure 11 shows the decrease in β, the resultant force angle relative to the surface normal, as the resultant force rotates toward the surface normal (see Figure 3).

4.3 Cutting Temperature

As noted, the cutting temperature was measured using an infrared camera during the slotting cuts. For each slot, the temperate map was analyzed and the maximum temperature achieved at the tool-workpiece interface was recorded. These temperature values were then evaluated as the tool wear increased with additional slots and machining time. An example temperature map is presented in Figure 12. The machining setup is displayed on the left and the corresponding temperature profile, with the setup features also identified, is shown on the right. The results from three digital temperature "probes" are also reported in the figure. It is seen that the temperatures at these three probes are {285, 318, and 210} °C. Other high temperature areas are also observed in the plot. These identify the hot chips that have been ejected from the cut. These temperatures were not considered. Figure 13 shows the change in maximum cutting temperature with slot number. As expected, the temperature increases substantially with FWW. In comparison with Figure 5, both the temperature and FWW increase by approximately the same percentage from slot 1 to slot 8.

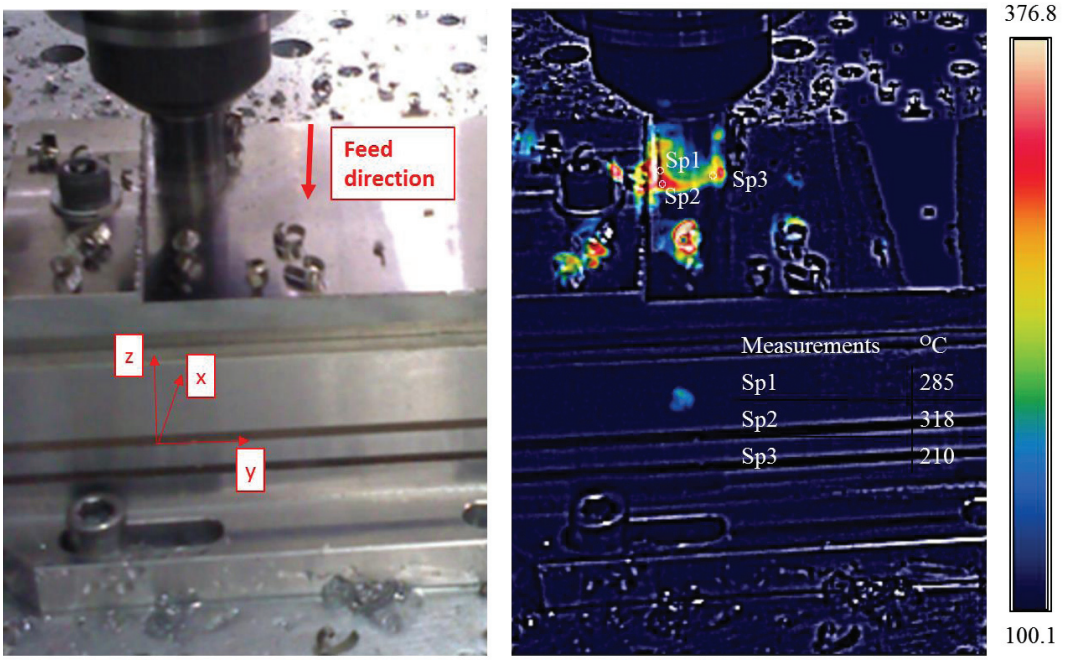

Figure 12. Left (machining setup) and (right) example temperature map. The color bar units are °C.

4.4 Surface Finish

The surface finish was evaluated by extracting a line scan in the feed direction from the central measurement identifed in Figure 2. The tip/tilt from the best fit plane to the height data was removed prior to extracting the line scan, but no other filtering was applied. An example result is displayed in

Figure 14. It is seen that the surface becomes more irregular as wear progresses. The peak-to-valley height also increases. However, the average roughness value, Ra, does not reflect the variation in surface character. This suggests that other surface parameters and evaluation criteria may be more appropriate, but the selection of alternative parameters was not considered as part of this study. This will be addressed in follow-on research.

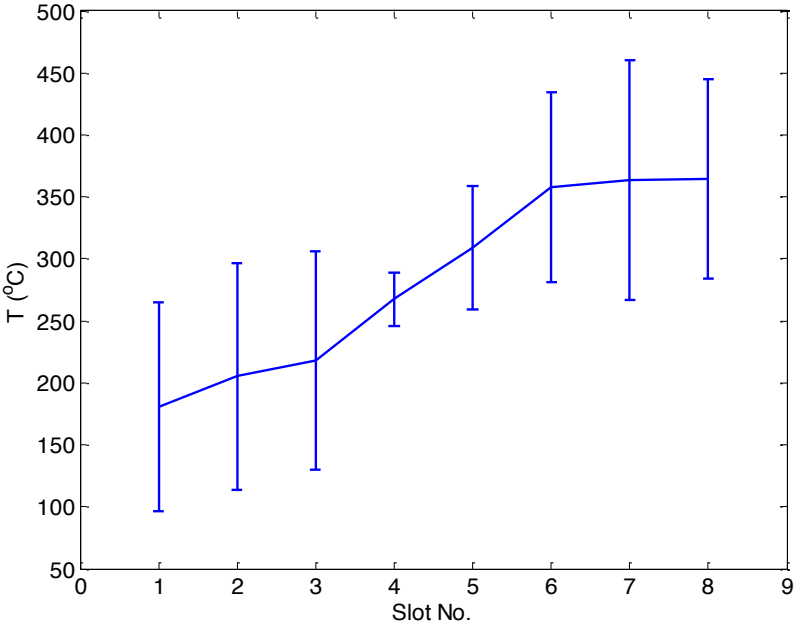

Figure 13. Change in cutting temperature with tool wear.

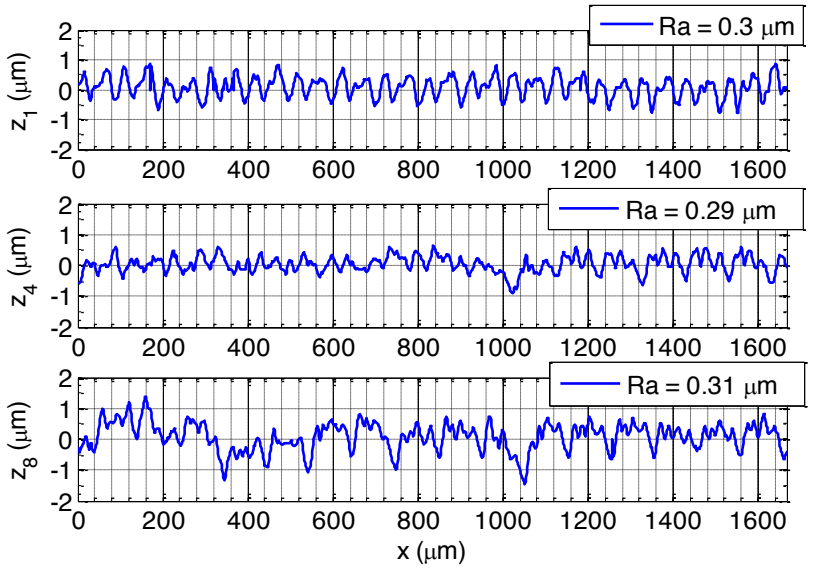

Figure 14. (Top) Surface height, *z*, as a function of scan length, *x*, after slot 1. (Middle) Surface height after slot 4. (Bottom) Surface height after slot 8.

5 Discussion

In order to relate: 1) the change in process behavior due to increasing tool wear; to 2) machining productivity, the following exercise was completed. Using the cutting force coefficients, a stability diagram was generated for a selected radial depth of cut. To determine the stability diagram, the system dynamics were defined by the tool point frequency response function (or FRF) that was measured using impact testing, where an instrumented hammer is used to excite the tool point and the response is measured at the same location using a low mass accelerometer. The FRF measurements are displayed in Figure 15. For each stability lobe diagram, the critical stability limit was identified; this is the axial depth of cut that is stable at all spindle speeds, $b_{lim,cr}$. Using the selected radial depth, a, corresponding axial depth, $b_{lim,cr}$, feed per tooth, f_t, number of teeth, N_t, and spindle speed, Ω, the mean MRR was calculated using $\text{MRR} = ab_{lim,cr}f_tN_t\Omega$. The radial depth was varied to determine the corresponding $b_{lim,cr}$. The feed per tooth was 0.1 mm/tooth, the number of teeth was 1, and the spindle speed was 835 rpm in all cases. The variation in $b_{lim,cr}$ and MRR with radial depth for the new and worn cutting conditions is presented in Figure 16. The subsequent reduction in productivity with tool wear is observed. Note that these two curves bound the productivity. As the tool wears (see Figure 5), the specific cutting force increases (see Figure 10). The increased specific cutting force results in a smaller critical stability limit. Intermediate wear states appear between the two curves.

It is observed that, although the FWW continues to increase in slots 6-8 (Figure 5), the cutting force coefficients (Figures 8-10), force angle (Figure 11), and cutting temperature (Figure 13) remain nearly constant. The authors speculate that these values tend to "saturate" above a certain FWW. This effect will be further investigated in follow-on testing.

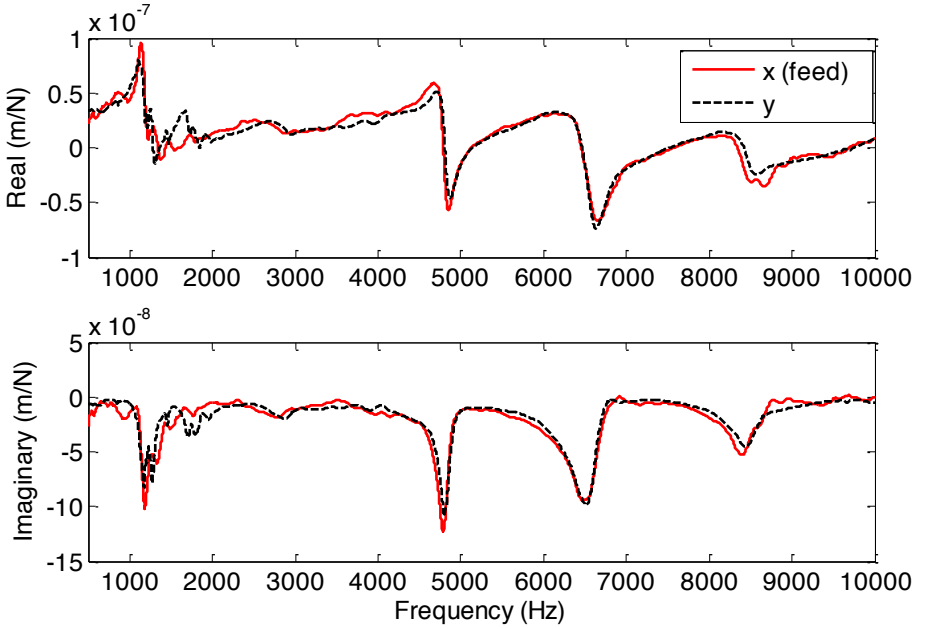

Figure 15. Tool point FRF in the *x* (feed) and *y* directions. (Top) real part and (bottom) imaginary part.

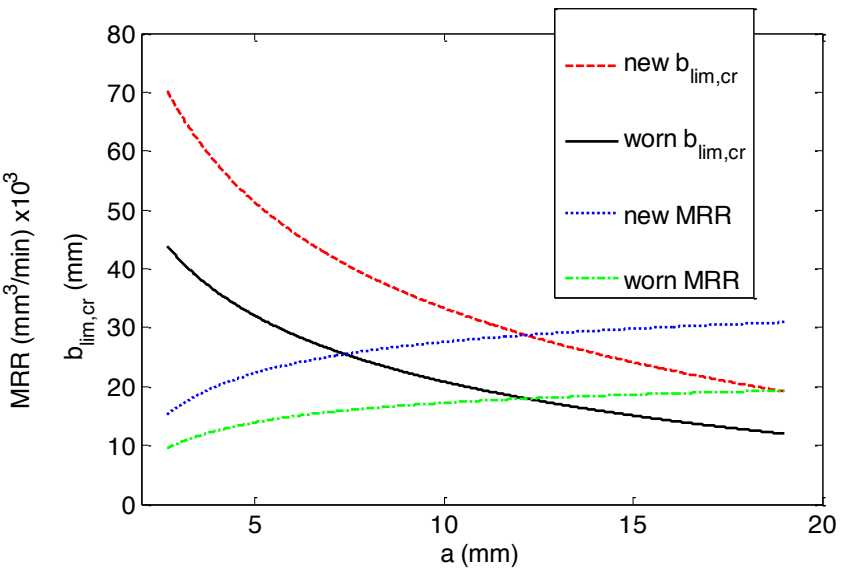

Figure 16. Variation in MRR and $b_{lim,cr}$ with radial depth of cut for new and worn insert states.

6 Conclusions

In this paper, experimental results were presented for flank wear width, cutting force, temperature, and surface finish as tool wear increased in titanium (Ti6Al4V) milling. The variation in these important process indicators was presented for four repeated trials of eight slotting cuts each as the wear progressed from a new tool condition to a worn state. Using the force data, cutting force coefficients were determined using a nonlinear optimization algorithm. These coefficients were then used together with the tool point dynamics to predict the process stability. The achievable chatter-free material removal rate was then computed for both the new and worn tool conditions. In this way, the variation in productivity was related to the wear state. It was shown that the process productivity decreased through the combined limitations imposed by chatter and tool wear. As anticipated, the productivity reduced with increased wear. However, it was also observed that the cutting force coefficients and temperature reached approximately steady-state values as the flank wear width increased beyond a value that would traditionally be considered to mark the end of tool life.

7 Acknowledgements

This material is based upon work supported by the National Science Foundation under Grant No. CMMI-1561221.

References

Abele E and Fröhlich B. High speed milling of titanium alloys. *Advances in Production Engineering and Management* 2008; 3: 131-140.

Altintas Y. *Manufacturing Automation: Metal Cutting Mechanics, Machine Tool Vibrations, and CNC Design.* New York: Cambridge University Press, 2012.

Campatelli G and Scippa A. Prediction of milling force coefficients for Aluminum 6082-T4. *Procedia CIRP* 2012; 1: 563-568.

Castejóna M, Alegrea E, Barreiroa J, and Hernández, LK. On-line tool wear monitoring using geometric descriptors from digital images. *International Journal of Machine Tools and Manufacture* 2007; 47(12-13): 1847-1853.

Coleman TF and Li Y. On the convergence of interior-reflective Newton methods for nonlinear minimization subject to bounds. *Mathematical Programming* 1994; 67: 189-224.

Hartung P, Kramer B, and von Turkovich B. Tool wear in titanium machining. *Annals of the CIRP* 1982; 31(1): 75-80.

Hong S, Markus I, and Jeong WC. New cooling approach and tool life improvement in cryogenic machining of titanium alloy Ti-6Al-4V. *International Journal of Machine Tools and Manufacture* 2001; 41(15): 2245-2260.

Kuttolamadom M., Mears L, and Kurfess T. On the volumetric assessment of tool wear in machining inserts with complex geometries Part I: Need, methodology, and standardization. *Journal of Manufacturing Science and Engineering* 2012; 134(5): 051002 (8 pages).

Kuttolamadom M., Mears L, and Kurfess T. On the volumetric assessment of tool wear in machining inserts with complex geometries Part II: Experimental investigation and validation on Ti-6Al-4V. *Journal of Manufacturing Science and Engineering* 2012; 134(5): 051003 (9 pages).

Niaki F, Ulutan D, and Mears L. Stochastic tool wear assessment in milling difficult to machine alloys. *International Journal of Mechatronics and Manufacturing Systems* 2015; 8(3-4) DOI: 10.1504/IJMMS.2015.073090.

Nouari M and Ginting A. Wear characteristics and performance of multi-layer CVD-coated alloyed carbide tool in dry end milling of titanium alloy. *Surface and Coatings Technology* 2006; 200(18-19): 5663-5676.

Remadna M and Rigal JF. Evolution during time of tool wear and cutting forces in the case of hard turning with CBN inserts. *Journal of Materials Processing Technology* 2006; 178(1-3): 67-75.

Schmitz TL and Smith KS. *Machining Dynamics: Frequency Response to Improved Productivity.* New York: Springer Science & Business Media, 2008.

Sun S, Brandt M, and Mo J. Evolution of tool wear and its effect on cutting forces during dry machining of Ti-6Al-4V alloy. *Proc. IMechE Part B: Journal of Engineering Manufacture* 2014; 228(2): 191-202.

Tlusty J. *Manufacturing Processes and Equipment*. Upper Saddle River, NJ: Prentice Hall, 1999.

Zelenski P. http://www.mmsonline.com/articles/consistency-is-key-to-titanium, 2012.